Department of Meteorology

DIAMET

National Centre for Atmospheric Science
NATURAL ENVIRONMENT RESEARCH COUNCIL

NATURAL ENVIRONMENT RESEARCH COUNCIL

Storm risk mitigation

University of Reading

Multiple mesoscale airstreams within regions of strong winds in extratropical cyclone Friedhelm

Oscar Martínez-Alvarado | Laura Baker | Sue Gray | John Methven | Bob Plant

o.martinezalvarado@reading.ac.uk

Introduction

The jet across the North Atlantic was exceptionally strong throughout December 2011. During the period with strongest baroclinicity a succession of fast-moving storms crossed the UK. Cyclone Friedhelm, which hit Scotland on 8 December 2011 (Fig. 1 a), was the most severe of these storms. The structure of this storm, and the location of the strongest winds, led to speculation that it contained a sting jet. This is a mesoscale descending airstream that can cause strong near-surface winds in the dry slot of cyclones, a region not usually associated with strong winds (Browning, 2004; Clark et al., 2005).

In this contribution we present a detailed analysis of the material origin of air masses constituting regions of strong low-level winds near the cloud head tip in cyclone Friedhelm. The analysis consists of numerical simulations using the operational Met Office weather forecast model supplemented by trajectory analysis and diagnostics of atmospheric instabilities. The analysis is supported by observations from the FAAM research aircraft which flew through the cyclone during the second DIAMET (DIAbatic influences on Mesoscale structures in ExtraTropical storms) field campaign - the first research flight through a sting-jet storm to the authors' knowledge.

Evaluation of the model simulation against observations

- Satellite imagery (Fig. 1 a) shows a well-defined cloud head hooking around the cyclone centre, with cloud banding at the cloud head tip.
- The frontal system and intensity of the cyclone is shown in the Met Office analysis (Fig. 1 b): the separation between isobars around the low pressure centre corresponds to geostrophic winds of over 40 m s $^{-1}$.
- The synoptic situation at T+12 of the model simulation (Fig. 1 c) corresponds remarkably well with the analysis chart in terms of the depth of the cyclone (957 hPa), and the location of the low-pressure centre and surface fronts.
- Dropsondes and in-situ measurements sampled some of the strongest winds (Fig. 2 a and d) .
- The model simulation at 1200 UTC shows a similar structure to the dropsonde observations (Fig. 2 b and c). However, there are some differences: the strong winds in the model extend up to 600 hPa compared with 800 hPa in the observations; the model is drier at low levels but has cloudy air extending up to around 400 hPa, compared with 500 hPa in the observations.
- At 1500 UTC the model underestimates horizontal wind speed for the first part of the flight (Fig. 2 e) but agrees with the observations after this. The model cloud corresponds well with the observations (Fig. 2 e) but has a wider cloudy region than was observed.
- Distinct air masses identified by trajectory analysis correspond to changes in observed CO concentrations (Fig. 2 f), consistent with the different origin location of each air mass.

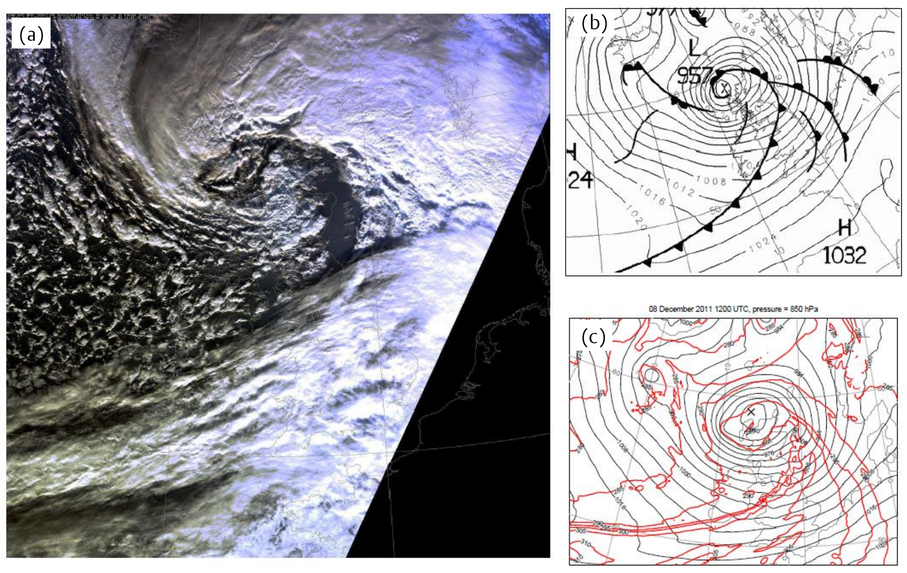

Figure 1: (a) High-resolution visible satellite image at 1215 UTC 8 December 2011 (courtesy NERC Satellite Receiving Station, Dundee University). (b) Met Office analysis valid at 1200 UTC 8 December 2011 (Crown copyright). (c) Model-derived mean sea level pressure (black contours) every 4 hPa and 850 hPa equivalent potential temperature (red contours) every 5 K at 1200 UTC 8 December 2011 (T+12). X marks the position of the cyclone centre.

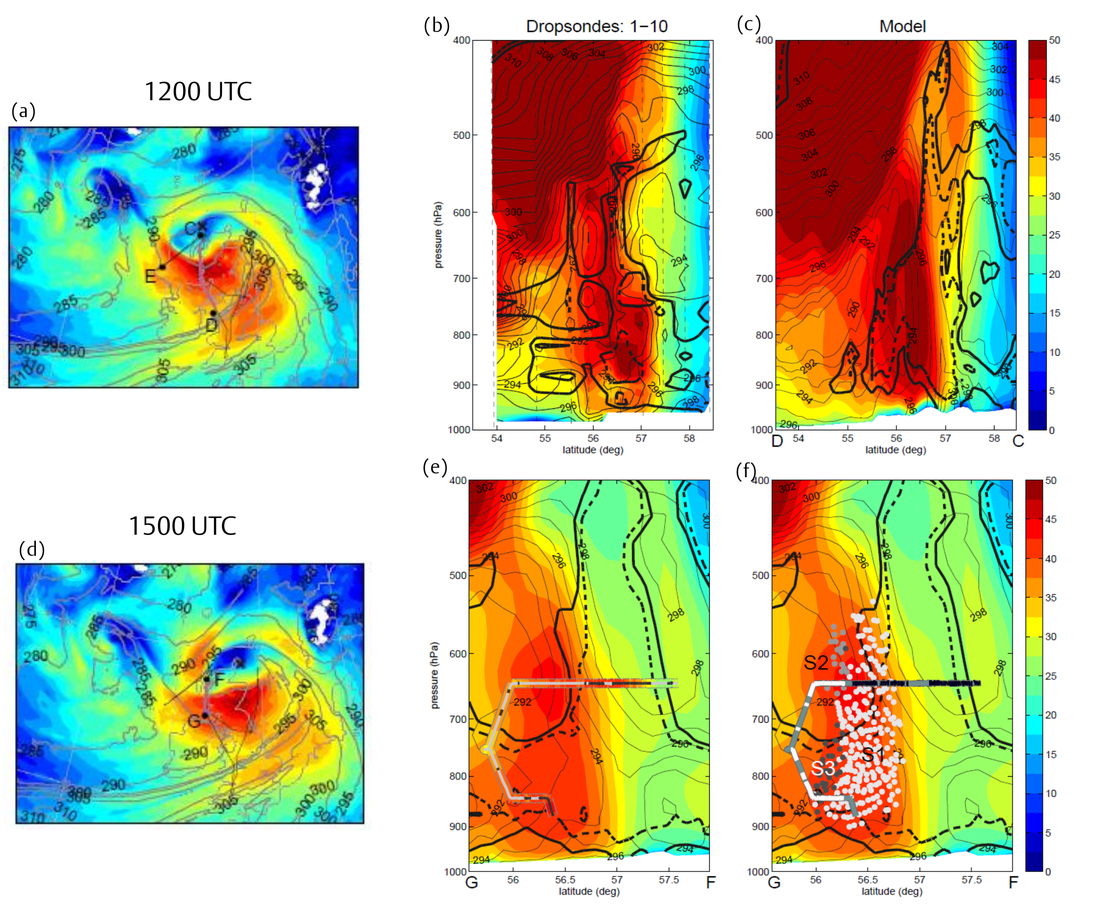

Figure 2: Horizontal and vertical cross-sections of ground-relative wind strength (in m s^{-1}). (a) shows wind speed at 850 hPa with grey contours of θ_e (K) at the same level, at 1200 UTC 8 December 2011. Also shown is the flight track (black lines) and location of the dropsonde section in (b) (purple line). (d) as in (a) but for 1500 UTC and with the purple line showing the position of in-situ measurements shown in (e). (b) shows the dropsonde observations of wind speed, θ_e (thin black contours) and 80 % and 90 % relative humidity with respect to ice (bold and dashed black contours) between 1130 UTC and 1234 UTC. (c) shows the equivalent model section at 1200 UTC. (e) and (f) show the model section between F and G in (d). In (e) the pipe shows in-situ measurements of wind speed (outer colours) and RH (inner colour; grey: RH < 80 %, black: RH > 80 %). In (f) the pipe shows observed CO concentration (black: up to 115 ppb; grey: 115-120 ppb; white: above 120 ppb). Coloured dots in (f) correspond to the three air streams identified from trajectory analysis: S1 (CCB, white), S2 (sting jet, light grey), S3 (CCB2, dark grey).

Properties of air masses associated with strong winds

Trajectories were computed back from regions of strong winds at 1300 UTC, 1600 UTC and 1800 UTC. Only the 1600 UTC trajectories are shown here but trajectories with similar characteristics were also found at other times. Three distinct trajectory sets were identified. Based on the behaviour of these trajectory sets, they were classified as follows:

- S1: cold conveyor-belt (CCB1)
- S2: sting jet (SJ)
- S3: cold conveyor-belt (CCB2)

- CCB trajectories (Fig. 3 a and c) remain mostly at low-levels, while SJ trajectories (Fig. 3 b) originate at higher levels.
- SJ trajectories have a period of descent before reaching their maximum wind speed, while CCB trajectories ascend during this time (Fig. 4 a).
- SJ trajectories retain a constant θ_e, while CCB trajectories have increasing θ_e, consistent with mixing (Fig. 4 b).
- SJ trajectories have a rapid decrease in RH during descent, while CCB trajectories remain moist (Fig. 4 c).
- All trajectory sets show a similar increase in Earth-relative wind speed (Fig. 4 d), but SJ trajectories have a much later increase in system-relative winds than CCB trajectories, corresponding to the descent period (Fig. 4 e).
- CCB trajectories are predominantly associated with stable air, with small numbers of trajectories associated with CI and CSI, and only very few with II (Fig. 5 a and c).
- SJ trajectories are characterised by much more unstable air (Fig. 5 b). Around 30 % of S2 trajectories are associated with II for a period of 5-6 hours. For around 6 hours more than 50 % of S2 trajectories are associated with CSI. This supports the link between CSI release and sting jets found by, e.g., Gray et al. (2011).

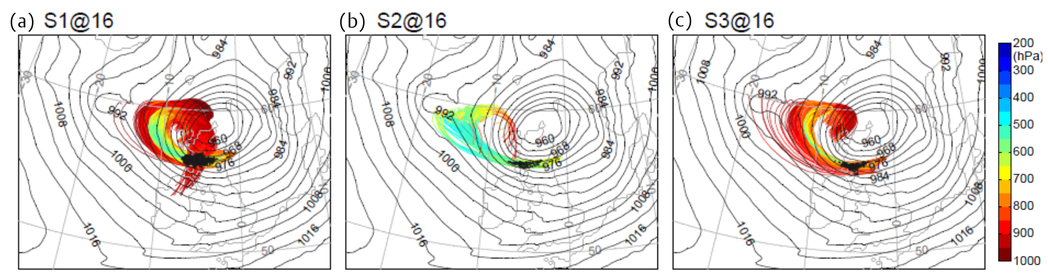

Figure 3: Mean sea-level pressure at 1500 UTC. Backward trajectories converging into regions of strong winds at 1600 UTC coloured by pressure, classified as (a) S1, (b) S2 and (c) S3. Black dots represent the position of the trajectory air parcels at 1500 UTC.

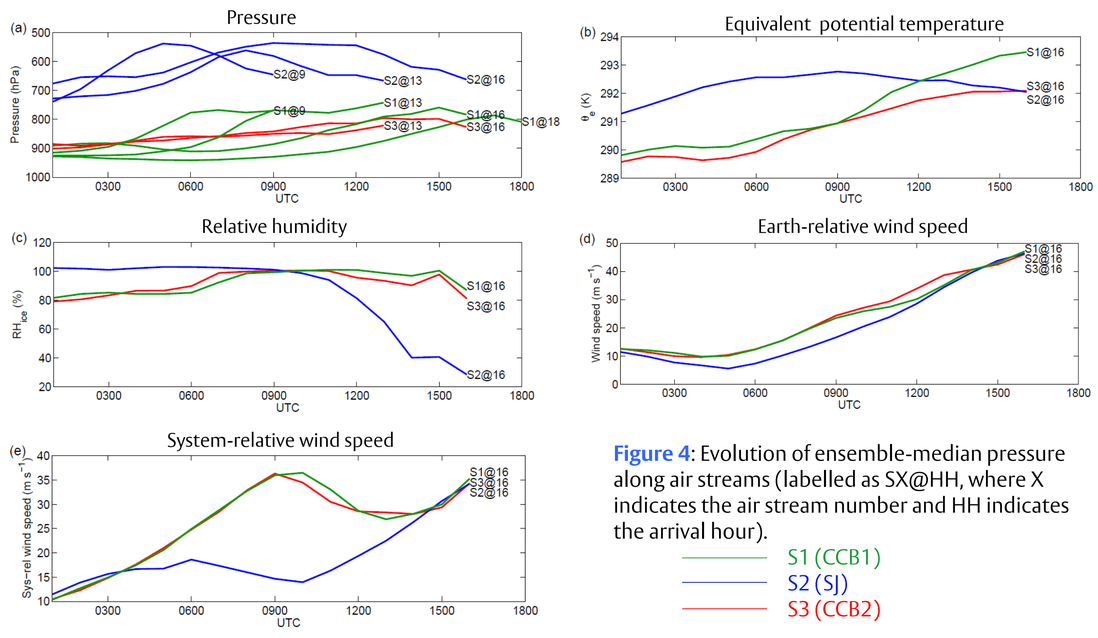

Figure 4: Evolution of ensemble-median pressure along air streams (labelled as SX@HH, where X indicates the air stream number and HH indicates the arrival hour).

S1 (CCB1)
S2 (SJ)
S3 (CCB2)

Conclusions

- We have shown that the strong winds south of the cyclone centre in extratropical cyclone Friedhelm can be attributed to 3 distinct air masses: two defined as cold conveyor belts and one as a sting jet.
- The vertical structure of the model cyclone compares well with observations.
- The distinction between the air masses is consistent with observations of different CO concentrations.
- The SJ trajectories show descent, drying and system-relative acceleration just before they reach the low-level strong winds and have nearly constant θ_e; the CCB trajectories accelerate earlier, remain moist, ascend and have increasing θ_e .
- SJ trajectories are associated with inertial instability and conditional symmetric instability; CCB trajectories are predominantly stable.

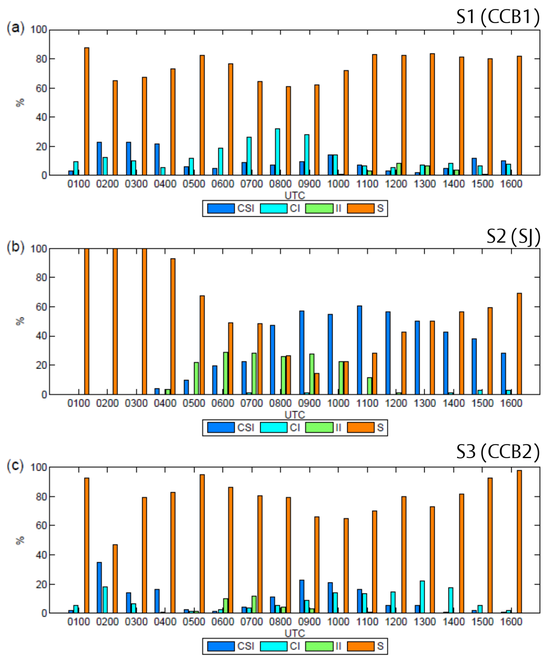

Figure 5: Diagnosis of instabilities along trajectories for each air stream with arrival time 1600 UTC. The histogram shows the percentage of trajectories in each air stream satisfying each instability or stability criteria at each hour. Colours represent conditional symmetric instability (CSI, dark blue), conditional instability (CI, light blue), inertial instability (II, green) and stability (S, orange). Instability types were diagnosed using moist potential vorticity, absolute vorticity and moist static stability, following the method used by Baker et al. (2013).

References

Baker, L. H., S. L. Gray, P. A. Clark (2013): Idealised simulations of sting jet cyclones. *Q. J. R. Met. S.*, DOI:10.1002/qj.2131 (In Press).

Browning, K. A., 2004: The sting at the end of the tail: Damaging winds associated with extratropical cyclones. *Q. J. R. Met. S.*, 130, 375–399.

Clark, P. A., K. A. Browning, and C. Wang, 2005: The sting at the end of the tail: Model diagnostics of fine-scale three-dimensional structure of the cloud head. *Q. J. R. Met. S.*, 131, 2263–2292.

Gray, S. L., Martinez-Alvarado, O., Baker, L. H. and Clark, P. A. (2011): Conditional symmetric instability in sting-jet storms. *Q. J. R. Met. S.*, 137 (659), 1482-1500. ISSN 1477-870X